Spermidine Modulated Ribonuclease Activity Probed by RNA Plasmon Rulers

Lynell R. Skewis and Björn M. Reinhard*

Department of Chemistry, Boston University, Boston, Massachusetts 02215

ABSTRACT

We extend the scope of nanometer distance measurements based on coupled pairs of gold nanoparticles, or plasmon rulers, to individual RNA molecules. These sensors were used to monitor the influence of spermidine on the cleavage kinetics of RNA by ribonuclease A. Time-resolved cleavage experiments of individual RNA plasmon rulers reveal transiently stabilized RNA sub-populations at increased spermidine concentrations that indicate spermidine-induced stabilization of weak secondary and tertiary structural elements.

Interactions between counterions and RNA are critical for the formation of stably folded RNA structures because they ease the electrostatic repulsion of closely packed backbone phosphates.[1,2] Divalent metal ions, magnesium (Mg^{2+}) in particular, are crucial for the correct folding of RNAs.[5,6] However, in cells metal ions are not the only counterions that interact with RNA. Polyamines such as spermine, spermidine, and putrescine also interact with nucleic acids, and it has been suggested that they subtly modulate RNA-folding transitions due to their higher charges and flexible structures.[7] Indeed, it has been shown that spermidine induces RNA-folding[8,9] and stabilizes RNA duplexes.[4] These spermidine-induced structural effects can be expected to have implications for protein-RNA interactions as well. The specific mechanisms of protein-RNA interactions,[10] their regulation, and the role of higher charged polycations such as spermidine in these interactions are still poorly understood.

The development of a mechanistic understanding of these processes would benefit from dynamic studies, ideally at the single molecule level, where it becomes possible to detect transient intermediates and multiple reaction pathways.[11] A method that has proven especially useful in investigating the dynamics in biological systems is single molecule fluorescence resonance energy transfer (FRET)[12] between two organic dyes. The limited photostability and brightness of the fluorescent dyes, however, motivates the development of alternative nonfluorescent-based technologies.
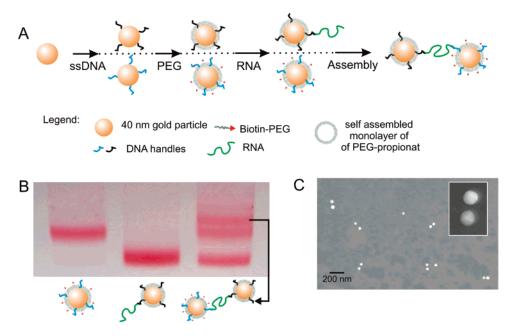
Gold nanoparticles have collective electron oscillations (plasmons) in the visible range of the spectrum. Because their signal is based on light scattering, gold nanoparticles do not blink nor bleach and are many orders of magnitude brighter than conventional organic dyes.[13] A wide range of biological sensing and detection schemes utilize these advantageous optical properties of gold nanoparticles and nanorods.[14−18]

One such scheme exploits the distant dependent coupling[19−25] of the plasmons of two close by particles. Individual pairs of double-stranded DNA-linked noble metal nanoparticles have been shown to act as dynamic molecular rulers for distances in the 1−70 nm range.[20,26,27] The resonance wavelength of paired gold nanoparticles red-shifts, and the scattering intensity increases as the particles get closer to each other. Their brightness, long lifetime, nonblinking, and chemical stability make plasmon rulers a good choice for highly parallel in vitro single molecule experiments with high temporal resolution for all applications that can tolerate the presence of the probes.[26]

The applicability of plasmon rulers has been limited to measuring distances and distance changes in double-stranded DNA. But herein, we introduce RNA plasmon rulers to the intriguing field of RNA biology. Our specific aim was to investigate the modulation of the activity of ribonuclease A (RNase A) by the triamine spermidine using plasmon rulers. RNase A cleaves only single-stranded RNA at the 3′ of cytosine (C) and uracil (U) residues. Such cleavage events lead to a clear drop in scattering intensity of the plasmon rulers. Plasmon rulers are particularly well suited for these studies as they facilitate the investigation of isolated RNA molecules free of perturbations through spermidine-induced RNA precipitation and aggregation.[28,29]

Synthesis and Characterization of RNA Plasmon Rulers. RNA dimers were synthesized by an RNA-programmed self-assembly process (for a schematic see Figure 1A and refer to Supporting Information). Using a sequential ligand exchange reaction, we first functionalized 40 nm gold particles with trithiolated single-stranded DNA (ssDNA) handles in a ratio of 1:25 (gold nanoparticle/DNA). Subsequently, the surface was passivated with a self-assembled monolayer of short thiolated carboxy-terminated polyethyleneglycols (thiol-(EG)$_7$-propionate). This passivation was required to stabilize the particles in salt buffers representing

* Corresponding author. E-mail: bmr@bu.edu.

Figure 1. Assembly and characterization of RNA plasmon rulers. (A) 40 nm gold particles are functionalized with single-stranded DNA (ssDNA) and pegylated with short thiol-propionate-PEGs. One particle is functionalized with biotinylated PEGs as well. Then RNA is annealed to one of the particles. Finally, the particles are combined to self-assemble. (B) Purification of plasmon rulers through gel electrophoresis. (C) TEM micrograph of isolated RNA plasmon rulers on a protein functionalized TEM grid. At higher magnification (inset), the separation between the particles is evident.

biologically relevant conditions. For one of the particles, small amounts of biotinylated polyethyleneglycols (PEGs) were added to the thiol-PEG-propionate to facilitate the binding of the particle to NeutrAvidin functionalized surfaces. In vitro transcribed RNA (total length: 155 nucleotides) that contains complementary sequences with the handles (22 nucleotides) at its 5′ and 3′ end was then annealed to the first handle. The RNA was reacted with the gold particles in a 1:30 (gold nanoparticle/RNA) ratio. The RNA functionalized particles were thoroughly cleaned and combined with the particles carrying the second handle. This reaction mix was finally analyzed for dimer formation using gel-electrophoresis.
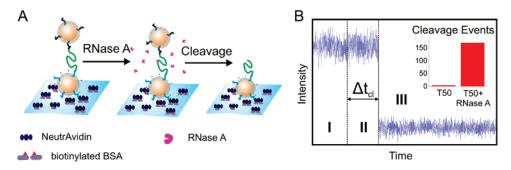
The gel shown in Figure 1B contains particles functionalized with one of the handles (outer left lane), particles with the other handle annealed to RNA (middle lane), and the reaction mix (outer right lane). Only the reaction mix contains a third band indicative of dimer formation that runs slightly slower than the RNA functionalized particles. The tentative dimer band was isolated through electroelution[26] and inspected by transmission electron microscopy (TEM) (Figure 1C). After electroelution, the preparations typically contained ~50% dimers. This is less than observed before for DNA plasmon rulers (~75%).[26] We attribute this finding to the fact that RNA is less stable than DNA, due especially to spontaneous self-cleavage.[30]

The individual particles in the dimers shown in the TEM micrograph in Figure 1C are separated by a distinct gap. This proves that the particles are indeed tethered by the biopolymer as opposed to sticking together nonspecifically. The interparticle distances observed for surface-bound dimers in the TEM however have no obvious correspondence to the equilibrium distance in aqueous solution. Because the

persistence length of single-stranded RNA (~0.8−0.9 nm)[31,32] is significantly shorter than that of the double-stranded DNA (~53 nm)[33] used in previous plasmon rulers, it was not clear a priori if the RNA in the space between the particles is actually accessible to RNA-binding enzymes.

To test the accessibility of the RNA tether, we studied the cutting efficiency of RNase A when applied to RNA plasmon rulers.[34] To that end we immobilized the RNA plasmon rulers with one particle on the surface of a NeutrAvidin-coated glass flow chamber (see Figure 2A) and monitored the intensity of the rulers during incubation with RNase A using darkfield microscopy.[20,35] A 40× (NA = 0.65) objective in combination with an enhanced charged coupled device detector allowed us to record scattering intensities of many plasmon rulers in parallel (~60 in a ~120 × 120 μm^2 field of view) at a frame rate of 96 Hz. Cleavage of the RNA tether between the particles leads to an abrupt drop in the scattering intensity as the dimer is converted into a monomer (see Figure 2B). Only the surface-bound particle remains visible on the surface, while the second particle diffuses into solution. We acquired a control by flushing the chamber with only T50 (50 mM NaCl, Tris·HCl, pH 8) upon which we observed no indication of RNA cleavage. When we flushed the chamber with RNase A in T50 at a concentration of 1 nM, we observed many rapid intensity drops indicating RNA cleavage. The total number of events obtained for three experiments (of each condition) are histogrammed in the inset in Figure 2B. The effective cleavage of RNA through RNase A proves that the RNA is accessible and that the cleavage is enzyme specific.

The ratio of ~25 DNA handles per 40 nm gold nanoparticles used here corresponds to a surface density of DNA of 1 molecule/201 nm^2 at the most. For each RNA molecule

Figure 2. Plasmon ruler RNase A cleavage assay. (A) The RNA plasmon rulers are bound to the surface of a glass flow chamber using a BSA (bovin serum albumin)−Biotin−NeutrAvidin surface chemistry. Upon addition of RNase A, the RNA tether is cleaved, and the dimer converted into a monomer. (B) Single RNA plasmon ruler cleavage trajectory (recorded at 96 Hz). (I) The plasmon ruler is first incubated in buffer containing spermidine at defined concentrations (0 −5 mM), (II) the buffer is exchanged with a 1 nM RNase A solution, causing (III) a strong drop in intensity upon RNA cleavage. Inset: Number of cleavage events for flushing with/without enzyme. Δt_{cl} is defined as the time between enzyme addition and cleavage.

annealed to a DNA handle, there are 25 available annealing sites on the second particle (surface area: 5027 nm^2). Given this low number of available binding sites and an overall decreased annealing efficiency close to surfaces,[36] the probability of formation of multiple tethers between the particles is low. In the case of DNA plasmon rulers with similar surface coverage with ssDNA, the fraction of particles with multiple tethers was estimated to be ∼5%.[26]
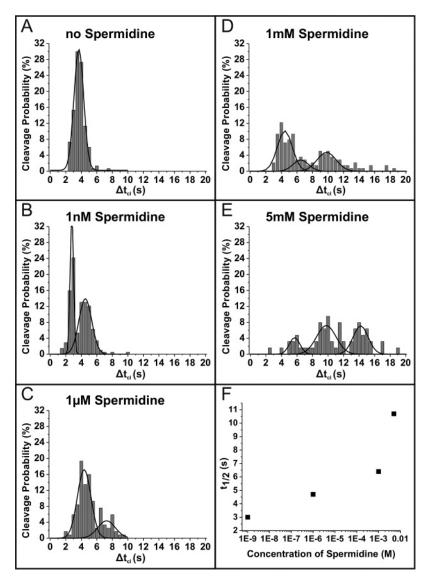
Structural Integrity of RNA Plasmon Rulers in the Presence of Polycations. To be able to quantify how RNA-bound spermidine modulates RNase A activity, we first had to probe the effect of polycations on the stability of the RNA plasmon rulers. The gold particles used in this study were functionalized with a PEG-propionate self-assembled mono-layer. Consequently, the surface charge is negative, which creates a repulsive interparticle potential that prevents the dimers from collapsing. Spermidine is positively charged under physiologic conditions and can bind nonspecifically to the gold particles. This poses the threat of a reduction of interparticle potential leading to the collapse of the dimer. It is not possible to detect RNA cleavage by RNase A when the dimer probe is in a collapsed state.

We therefore performed cleavage experiments (see Figure 2B and Supporting Information) for RNA that was prein-cubated with different polycations with charges ranging from +3 to +64. In addition to spermidine (nominal charge $q = +3$), we chose three different polyamidoamine (PAMAM) dendrimers: generation 0 (G0, $q = +4$), generation 1 (G1, $q = +8$), and generation 4 (G4, $q = +64$). After incubation with the polyamines, we determined the total number of cleavage events upon flushing the chamber with a 1 nM RNase A solution. For polyamines at a concentration of 2 μM, two experiments performed under otherwise identical conditions yielded 99 cleavage events for spermidine, 5 for G0, 12 for G1, and 0 for G4 dendrimers. While we observed efficient RNA cleavage for spermidine concentrations up to 5 mM, in the case of the dendrimers the cleavage probability dropped essentially to zero with increasing dendrimer concentration. Concurrent with the decrease in the total number of cleavage events, we observed more abrupt increases in intensity upon addition of the dendrimers (see Supporting Information, Figure S1). In the case of G4, almost

all dimers show this behavior at nanomolar concentrations. The intensity jumps are indicative of a fast decrease in the interparticle distance and indicate the collapse of the dimer or significant compaction of the RNA tether. With spermidine addition, we did not observe any systematic compaction even in concentrations up to 5 mM. The probes are stable in the presence of a wide range of concentrations of spermidine.

To further confirm the stability of the dimer probes in the presence of spermidine, we analyzed the gel-electrophoretic mobility of pegylated gold nanoparticles after incubations with increasing concentrations of spermidine (1 nM−1 mM) (see Supporting Information, Figure S2). The particles do not differ in their electrophoretic mobility. This observation indicates that spermidine incubation does not change the ζ-potential of the particles.[37] The high cleavage rates, minimal compaction rates and lack of observable changes in the electrophoretic mobility show that spermidine does not significantly influence the structural integrity of the RNA plasmon rulers. Therefore, the RNA tether is expected to be accessible over a wide spermidine concentration range.

Effect of Spermidine on Enzymatic RNA Degradation. Because of the strong signal caused by RNA cleavage, enzymatic RNA degradation is an ideal test system to quantify the influence of spermidine on RNA-binding enzyme activity. We measured the cleavage times, defined as time difference, Δt_{cl}, between the addition of RNase A and the observed cutting (see Figure 2B) for four different concentrations of spermidine (1 nM, 1 μM, 1 mM, 5 mM) and in the absence of spermidine. We recorded ∼120 trajectories for each spermidine concentration. The histo-grams in Figure 3A−E show the measured Δt_{cl}'s. On the basis of the cumulative Δt_{cl} distributions, we calculated the values of $t_{1/2}$, defined as the times at which half of the RNA degradation events had occurred (see Supporting Information, Figure S3). A plot of the value of $t_{1/2}$ versus spermidine concentration (Figure 3F) shows a clear increase in average cleavage time with spermidine concentration.

Spermidine binds both specifically and nonspecifically to RNA, where it reduces the negative charge density of the phosphate backbone.[7−9] Because the bovine RNase A used in these studies has a pKa value of 9.6, it is positively charged under our experimental conditions.[38] A reduction

Figure 3. Cleavage time (Δt_{cl}) distributions as function of spermidine (spd[3+]) concentration. (A) no spd[3+]; (B) 1 nM spd[3+]; (C) 1 μM spd[3+]; (D) 1 mM spd[3+]; (E) 5 mM spd[3+]. Gaussian fits mark potential sub-populations. Already a 1 nM spd[3+] concentration leads to a splitting of the Δt_{cl} distribution. With increasing spd[3+] concentrations, the cleavage events happen later and sub-populations with long lifetimes grow at the cost of fast sub-populations. (F) $t_{1/2}$ times (= time after which half of all the cutting events have occurred) vs concentration.
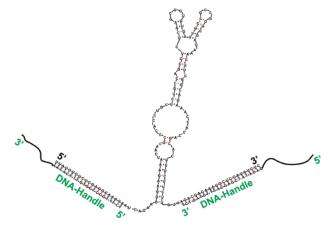
of the effective RNA charge decreases the nonspecific binding affinity of the positively charged RNase. The resulting overall lower binding affinity of the enzyme is one factor that can account for the shift of the Δt_{cl} distributions to longer times. Another factor that needs to be considered is the relative stabilization of potentially double-stranded regions in the RNA secondary structure versus single-stranded regions through spermidine.[3,4] Because RNase A can cleave only single-stranded RNA, a relative stabilization of duplexes equals an effective decrease of potential reaction sites for the enzyme.

We used Mfold[39] to analyze the secondary structure of the available RNA tether (sequences that anneal to DNA handles were omitted). The overall energetically lowest minimum ($\Delta G = -36$ kcal/mol) is shown in Figure 4. Mfold finds three other minima within only 3 kcal/mol of the lowest minimum. The shown structure is therefore only one of many possibilities among which the RNA fluctuates. Figure 4 illustrates, however, structural features common to several

minima. Many of the predicted secondary structures contain a long double-stranded region disrupted by internal bulges and internal loops and disembogue into two hairpins.

The RNA tethering of the particles in our plasmon rulers indeed contains double-stranded regions that could experience stabilization through spermidine. Venkiteswaran et al. report an increase in the melting temperature of 22.9 °C for a 15 bp long double-stranded RNA after addition of a 100 μM spermidine solution.[4] Individual RNA molecules spend increasingly more time in the duplex state as the melting temperature rises. Consequently, the increase in $t_{1/2}$ with growing spermidine concentration observed in our cleavage experiments can be explained by an increase in the number of RNA molecules with protected duplex regions.

Aside from an overall deceleration of the enzyme kinetics, Figure 3B−E shows distinct sub-populations when the RNA is preincubated with spermidine. While Figure 3A is well fit by a single Gaussian around $\Delta t_{cl} = 3.8$ s, increasing the concentration of spermidine causes sub-populations with

Figure 4. Predicted minimum secondary structure (with DNA handles). The structure contains multiple double-stranded regions that can be stabilized upon addition of spermidine.[3,4]
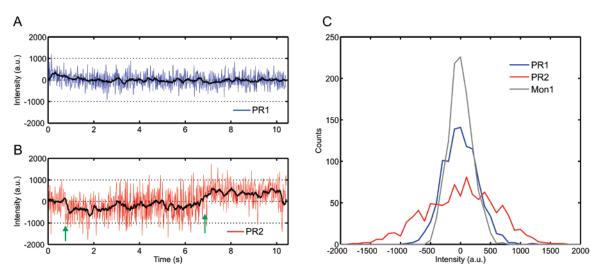
greater Δt_{cl} values to emerge. Already for 1 nM spermidine solution (Figure 3B), the Δt_{cl} distribution is no longer symmetric. Two sub-populations arise, one with a sharp peak centered at 2.7 s and a second, broader peak at 4.5 s. At 1 μM spermidine (Figure 3C), the fast subpopulation has vanished; instead, a third subpopulation emerges at around 7.2 s. At 1 mM spermidine (Figure 3D) a fourth, discrete subpopulation appears at 9.8 s. Finally, 5 mM spermidine (Figure 3E) shows two sub-populations centered at 9.8 and 14.2 s, and only marginal cleavage appears before 8 s.

We see no indication that the marked sub-populations are due to structurally uniform RNA species; however, the RNAs belonging to the individual sub-populations must share sufficient structural similarities to cause similar lifetimes. The species with longer lifetimes are transiently stabilized relative to RNAs of sub-populations with faster cleavage times. Depending on the spermidine concentration, the lifetimes of the later populations are extended by 1.8−8.5 s.

In the case of the 1 nM spermidine condition, a possible explanation for the bimodal distribution is that only a fraction (about one-half) of the RNA molecules are stabilized by spermidine. The remaining RNA tethers are not sufficiently protected, so the RNA is cleaved fast. Increasing spermidine concentration leads to the emergence of further sub-populations at later times. Additional stabilizations could arise for instance from a more effective protection of the RNA duplex region close to the DNA handles or the formation of specific tertiary structures, which can resist cleavage for longer times.[40] Better protected structures become available only after a certain number of spermidine molecules are bound to the substrate. The subsequent appearance of discrete sub-populations indicates some cooperativity between the RNA-bound spermidine molecules in their protection mechanism leading to distinctly stabilized states.

We also performed traditional ribonuclease protection assays for the RNA with the handles annealed (but without the gold nanoparticles) to verify if the transiently stabilized sub-populations are apparent in the bulk assay. Following standard procedures, RNA in varying salt and spermidine conditions was incubated with the enzyme for 1 min before the enzyme was heat deactivated and the mix loaded into a 15% polyacrylamide/urea denaturing gel. The gel did not indicate any structural stabilization. We attribute this to the long time scale of the bulk protection assay, which prevents the detection of short-lived species. This underlines the inherent advantage of the RNA plasmon rulers that combine the advantages of single molecule detection with high temporal resolution.

Intensity Distributions of Individual RNA Plasmon Rulers. The primary goal of this work was to examine the effect of spermidine on RNase A cleavage kinetics. The RNA plasmon ruler approach combines high throughput with high temporal resolution at the single molecule level and was

Figure 5. Scattering intensities. The intensity trajectories for two individual RNA plasmon rulers PR1 and PR2 are shown in (A) and (B). Twenty point sliding averages are included as black lines to guide the eye. The scattering trajectory of PR2 exhibits transitions between different average intensity levels at times marked by arrows (see text). (C) Histogrammed scattering intensities are shown for PR1 and PR2 as well as for one monomer Mon1 (PR1 after enzymatic cleavage). While the intensity distributions for plasmon rulers are in general broader than for monomers, the width of the intensity distributions of the plasmon rulers vary significantly as shown here for PR1 and PR2. The intensity distribution of PR2 is broadened due to the existence of multiple average intensity levels in the scattering trajectory.

therefore the method of choice to probe and quantify the modulation of RNA cleavage rates through spermidine. Direct structural information of individual RNA molecules in the presence of spermidine was not necessary to achieve our goal. It is, however, feasible that the scattering intensity of individual RNA plasmon rulers can contain such structural information. Two representative scattering trajectories are shown in Figures 5A,B. Some scattering trajectories contain intensity variations as shown in Figure 5B that could reflect changes in the RNA end-to-end distance or orientation of the RNA plasmon ruler. Although the magnitude of the intensity shifts is close to the detection limit at the chosen frame rate of 96 Hz, they can still be detected if the dwell time at each intensity level is long enough. These shifts of the average intensities lead to a strong broadening of the intensity distributions of the plasmon rulers (compare PR1 and PR2 in Figure 5C). Interestingly, the intensity distributions broaden significantly with increasing spermidine concentration; the standard deviation averaged over 52 trajectories of identical length (1000 points, 10.41 s) for plasmon rulers increases from 261 (T50 buffer, no spermidine) to 358 counts (+37.1%) in 1 mM spermidine solution.

Different from recent single dye pair FRET experiments, the RNA in our experiment was not designed to undergo specific structural transitions. The RNA under investigation here has several close energetic (secondary and tertiary) minimum structures and fluctuates between these conformers. Single dye pair FRET experiments, however, are generally applied to systems with discrete transitions, such as docking[41] or hairpin ribozyme folding.[42] The presence of such discrete states clarifies structural transition detection. However, due to the limited working distance of FRET (the optimum working distance for typical dye pairs such as Cy3/Cy5 is on the order of 5 nm) the dyes must be strategically located on the nucleic acid. This requires profound knowledge of the underlying mechanisms. In contrast, our technique applies probes to the ends of the nucleic acid and is sensitive to a wider range of distance changes.[20,21] Thus, RNA plasmon rulers could be a generic tool for dynamic RNA studies where the detailed mechanism of structural changes is less well understood.

Conclusions. Using pairs of RNA-tethered 40 nm gold nanoparticles, or RNA plasmon rulers, we have analyzed the influence of spermidine on the cleavage kinetics of RNase A at the single molecule level. Because of their high temporal resolution and the ability to follow the cleavage of individual RNA molecules, the RNA plasmon rulers provide information about relative stabilities of weakly stabilized subpopulation and their lifetimes. We observe efficient RNA cleavage rates for all investigated concentrations (1 nM−5 mM). Time-resolved cleavage experiments (temporal resolution: ~10 ms) show that with increasing spermidine concentration, cleavage is delayed and discrete sub-populations with longer lifetimes emerge. We attribute this observation to the formation of RNA structures that are transiently stabilized against enzymatic degradation by spermidine. The lifetimes of the stabilized species are extended by 1.8−8.5 s, which makes their detection impossible in traditional ribonuclease protection assays. The reduction of RNase A cleavage rates and appearance of sub-populations that indicate transient structural RNA stabilization confirm that RNA-binding enzyme activity is regulated through spermidine-induced changes in the charge and structure of the RNA substrate. The plasmon rulers are able to retrieve otherwise obscured information about weak structural stabilizations. RNA−protein interactions are integral components of posttranscriptional gene regulation at the levels of RNA processing, transport, and translation, highlighting the potential relevance of the spermidine modulated regulation process.

Supporting Information Available: Materials and Methods and Figures S1−S3. This material is available free of charge via the Internet at http://pubs.acs.org.

References

(1) Misra, V. K.; Draper, D. E. *Biopolymers* **1998**, *48*, 113−135.
(2) Bloomfield, V. A.; Crothers, D. M.; Tinocco, I. *Nucleic acids: structures, properties, and functions*; University Science Books: Sausalito, CA, 1999.
(3) Plum, G. E.; Bloomfield, V. A. *Biopolymers* **1990**, *29*, 13−27.
(4) Venkiteswaran, S.; Vijayanathan, V.; Shirahata, A.; Thomas, T.; Thomas, T. J. *Biochemistry* **2005**, *44*, 303−312.
(5) Draper, D. E.; Misra, V. K. *Nat. Struct. Biol.* **1998**, *5*, 927−930.
(6) Misra, V. K.; Draper, D. E. *J. Mol. Biol.* **2002**, *317*, 507−521.
(7) Tabor, C. W.; Tabor, H. *Annu. Rev. Biochem.* **1984**, *53*, 749−790.
(8) Koculi, E.; Lee, N. K.; Thirumalai, D.; Woodson, S. A. *J. Mol. Biol.* **2004**, *341*, 27−36.
(9) Hammann, C.; Hormes, R.; Sczakiel, G.; Tabler, M. *Nucleic Acids Res.* **1997**, *25*, 4715−4722.
(10) Draper, D. E. *J. Mol. Biol.* **1999**, *293*, 255−270.
(11) Zhuang, X. W.; Bartley, L. E.; Babcock, H. P.; Russell, R.; Ha, T. J.; Herschlag, D.; Chu, S. *Science* **2000**, *288*, 2048−2051.
(12) Ha, T.; Enderle, T.; Ogletree, D. F.; Chemla, D. S.; Selvin, P. R.; Weiss, S. *Proc. Natl. Acad. Sci. U.S.A.* **1996**, *93*, 6264−6268.
(13) Yguerabide, J.; Yguerabide, E. E. *Anal. Biochem.* **1998**, *262*, 157−176.
(14) Elghanian, R.; Storhoff, J. J.; Mucic, R. C.; Letsinger, R. L.; Mirkin, C. A. *Science* **1997**, *277*, 1078−1081.
(15) Stone, J. W.; Sisco, P. N.; Goldsmith, E. C.; Baxter, S. C.; Murphy, C. J. *Nano Lett.* **2007**, *7*, 116−119.
(16) Haes, A. J.; Hall, W. P.; Chang, L.; Klein, W. L.; Van Duyne, R. P. *Nano Lett.* **2004**, *4*, 1029−1034.
(17) West, J. L.; Halas, N. J. *Annu. Rev. Biomed. Eng.* **2003**, *5*, 285−292.
(18) El-Sayed, I. H.; Huang, X. H.; El-Sayed, M. A. *Nano Lett.* **2005**, *5*, 829−834.
(19) Quinten, M.; Kreibig, U. *Appl. Opt.* **1993**, *32*, 6173−6182.
(20) Reinhard, B. M.; Siu, M.; Agarwal, H.; Alivisatos, A. P.; Liphardt, J. *Nano Lett.* **2005**, *5*, 2246−2252.
(21) Jain, P. K.; Huang, W. Y.; El-Sayed, M. A. *Nano Lett.* **2007**, *7*, 2080−2088.
(22) Wei, Q. H.; Su, K. H.; Durant, S.; Zhang, X. *Nano Lett.* **2004**, *4*, 1067−1071.
(23) Su, K. H.; Wei, Q. H.; Zhang, X.; Mock, J. J.; Smith, D. R.; Schultz, S. *Nano Lett.* **2003**, *3*, 1087−1090.
(24) Rechberger, W.; Hohenau, A.; Leitner, A.; Krenn, J. R.; Lamprecht, B.; Aussenegg, F. R. *Opt. Commun.* **2003**, *220*, 137−141.
(25) Fromm, D. P.; Sundaramurthy, A.; Schuck, P. J.; Kino, G.; Moerner, W. E. *Nano Lett.* **2004**, *4*, 957−961.
(26) Reinhard, B. M.; Sheikholeslami, S.; Mastroianni, A.; Alivisatos, A. P.; Liphardt, J. *Proc. Natl. Acad. Sci. U.S.A.* **2007**, *104*, 2667−2672.

(27) Sonnichsen, C.; Reinhard, B. M.; Liphardt, J.; Alivisatos, A. P. *Nat. Biotechnol.* **2005**, *23*, 741−745.

(28) Bloomfield, V. A. *Biopolymers* **1997**, *44*, 269−282.

(29) Widom, J.; Baldwin, R. L. *Biopolymers* **1983**, *22*, 1595−1620.

(30) Soukup, G. A.; Breaker, R. R. *RNA* **1999**, *5*, 1308−1325.

(31) Seol, Y.; Skinner, G. M.; Visscher, K. *Phys. Rev. Lett.* **2004**, *93*, 118102.

(32) Caliskan, G.; Hyeon, C.; Perez-Salas, U.; Briber, R. M.; Woodson, S. A.; Thirumalai, D. *Phys. Rev. Lett.* **2005**, *95*, 268303.

(33) Smith, S. B.; Cui, Y. J.; Bustamante, C. *Science* **1996**, *271*, 795−799.

(34) We verified that that the enzyme does not degrade the single-stranded DNA handles (data not shown).

(35) Sonnichsen, C.; Franzl, T.; Wilk, T.; von Plessen, G.; Feldmann, J.; Wilson, O.; Mulvaney, P. *Phys. Rev. Lett.* **2002**, *88*, 077402.

(36) Hagan, M. F.; Chakraborty, A. K. *J. Chem. Phys.* **2004**, *120*, 4958−4968.

(37) Hunter, R. *Zeta Potentials in Colloid Science: Principles and Applications*; Academic Press: London, 1988.

(38) Mora, P. T. *J. Biol. Chem.* **1962**, *237*, 3210.

(39) Zuker, M. *Nucleic Acids Res.* **2003**, *31*, 3406−3415.

(40) Ehresmann, C.; Baudin, F.; Mougel, M.; Romby, P.; Ebel, J. P.; Ehresmann, B. *Nucleic Acids Res.* **1987**, *15*, 9109−9128.

(41) Bokinsky, G.; Nivon, L. G.; Liu, S. X.; Chai, G. Q.; Hong, M.; Weeks, K. M.; Zhuang, X. W. *J. Mol. Biol.* **2006**, *361*, 771−784.

(42) Ha, T. J. *Biochemistry* **2004**, *43*, 4055−4063.

NL0725042